Applied Physics Letters

RESEARCH ARTICLE | MARCH 02 2017

A silicon microwire under a three-dimensional anisotropic tensile stress FREE

Xiaoyu Ji; Nicolas Poilvert; Wenjun Liu; Yihuang Xiong; Hiu Yan Cheng; John V. Badding ; Ismaila Dabo; Venkatraman Gopalan

Appl. Phys. Lett. 110, 091911 (2017)
https://doi.org/10.1063/1.4977852

CHORUS

29 May 2024 01:12:47

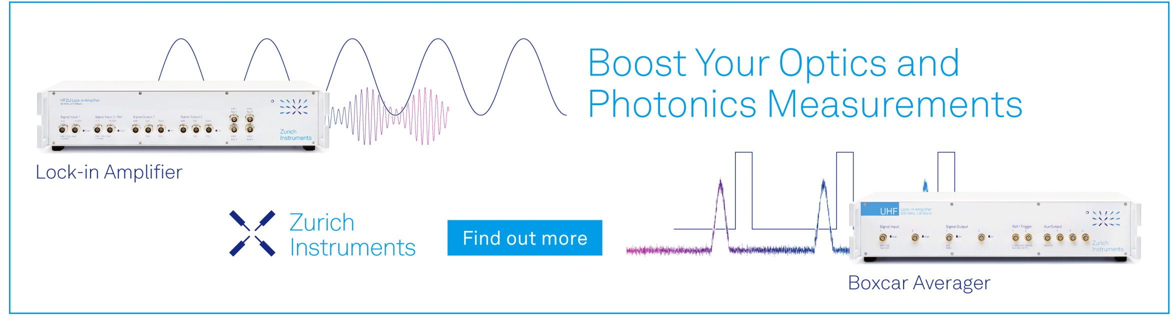

APPLIED PHYSICS LETTERS **110**, 091911 (2017)

A silicon microwire under a three-dimensional anisotropic tensile stress

Xiaoyu Ji,[1,2] Nicolas Poilvert,[1,2] Wenjun Liu,[3] Yihuang Xiong,[1,2] Hiu Yan Cheng,[2,4] John V. Badding,[1,2,4,5] Ismaila Dabo,[1,2] and Venkatraman Gopalan[1,2,a)]

[1]*Department of Materials Science and Engineering, The Pennsylvania State University, University Park, Pennsylvania 16802, USA*
[2]*Materials Research Institute, The Pennsylvania State University, University Park, Pennsylvania 16802, USA*
[3]*Advanced Photon Source, Argonne National Laboratory, Argonne, Illinois 60439, USA*
[4]*Department of Chemistry, The Pennsylvania State University, University Park, Pennsylvania 16802, USA*
[5]*Department of Physics, The Pennsylvania State University, University Park, Pennsylvania 16802, USA*

(Received 19 October 2016; accepted 18 February 2017; published online 2 March 2017)

Three-dimensional tensile stress, or triaxial tensile stress, is difficult to achieve in a material. We present the investigation of an unusual three-dimensional anisotropic tensile stress field and its influence on the electronic properties of a single crystal silicon microwire. The microwire was created by laser heating an amorphous silicon wire deposited in a 1.7 μm silica glass capillary by high pressure chemical vapor deposition. Tensile strain arises due to the thermal expansion mismatch between silicon and silica. Synchrotron X-ray micro-beam Laue diffraction (μ-Laue) microscopy reveals that the three principal strain components are +0.47% (corresponding to a tensile stress of +0.7 GPa) along the fiber axis and nearly isotropic +0.02% (corresponding to a tensile stress of +0.3 GPa) in the cross-sectional plane. This effect was accompanied with a reduction of 30 meV in the band gap energy of silicon, as predicted by the density-functional theory calculations and in close agreement with energy-dependent photoconductivity measurements. While silicon has been explored under many stress states, this study explores a stress state where all three principal stress components are tensile. Given the technological importance of silicon, the influence of such an unusual stress state on its electronic properties is of fundamental interest. *Published by AIP Publishing.* [http://dx.doi.org/10.1063/1.4977852]

29 May 2024 01:12:47

One of the most exciting aspects of semiconductor research is to use strain to engineer the electronic, optical, and optoelectronic properties of materials and ultimately improve device performance.[1,2] Silicon (Si), being the most important semiconductor in modern technologies, has been extensively studied for its strain tuning effects. Biaxial tensile strain has been applied in Si films through either capping with a silicon nitride layer[3,4] or growing on a silicon dioxide layer.[5] By patterning strained silicon-on-insulator films to relax the biaxial tensile strain, uniaxially tensile-strained Si nanowires are achieved.[5,6] Enhanced transport properties, band-gap modification,[7,8] enhanced light emission efficiency,[9] and electro-optic effects[4] can arise from strain tuning. Despite the ability to generate a variety of strain/stress states experimentally, anisotropic tensile stress in all three dimensions has not been reported or achieved for Si because either uniaxial or biaxial tensile stress will result in the other direction(s) of the material under compressive stress due to its positive Poisson's ratio.[10,11] In this work, we present studies of an unusual state of three-dimensional tensile stress in a single-crystal Si microwire derived from the thermal expansion mismatch with a surrounding glass capillary. Given the technological importance of silicon, a fundamental study of the consequences of such a stress state on its electronic properties should be of interest.

The single crystal Si microwire was created through transforming an amorphous Si wire using a laser crystallization technique.[12] The amorphous Si wire was deposited in a 1.7 μm silica glass capillary by high pressure chemical vapor deposition.[13] The as-deposited amorphous Si wire was then precisely irradiated by a 500 mW focused 488 nm argon ion laser, scanning at a speed of 1 mm/s along the wire. The method is described in detail in Ref. 12. Considering the unique geometry of our sample, we employed the synchrotron X-ray micro-beam Laue diffraction (μ-Laue) microscopy at the Advanced Photon Source of the Argonne National Laboratory to investigate the full strain state, characterized by the full strain tensor, of the microwire. As shown in Fig. 1(a), the focused X-ray beam, which has a size of $\sim$1.0 μm (vertical) $\times$ 0.6 μm (horizontal), is incident onto the fiber mounted 45° off the horizontal axis, and the diffracted X-rays from the sample are incident upon three amorphous Si area detectors. The detectors were well calibrated before all the experiments, and strain refinement uncertainties were minimized to the order of 10^{-4}.

It is well known that the orientation and unit-cell parameters can be determined from three independent X-ray reflections with known indices.[14] Similar to previously reported studies,[15] we performed energy-scanned monochromatic measurements on three widely separated, linearly independent reflections (one on each detector) from the same sample volume. The absolute lattice *d*-spacings, the Miller indices, and the locations of each diffraction peak on the detectors were then determined from the energy scan. Each reflection has two direction angles, so with three reflections, there are a total of six independent equations. The three measured *d*-spacings provide three additional independent equations; therefore, these measurements are sufficient to extract the full unit-cell parameters (a, b, c and α, β, γ) and the three crystal rotation angles.[14,15] Once the unit-cell parameters are known, the complete strain tensor can be obtained by the following:[16]

a)Electronic mail: vxg8@psu.edu

$$\begin{bmatrix} \varepsilon_{11} = \dfrac{a_1}{a_0}\sin\beta_1\sin\gamma_1 - 1 & \varepsilon_{12} = \varepsilon_{21} = -\dfrac{a_1}{2a_0}\sin\beta_1\cos\gamma_1 & \varepsilon_{13} = \varepsilon_{31} = \dfrac{a_1}{2a_0}\cos\beta_1 \\ * & \varepsilon_{22} = \dfrac{b_1}{b_0}\sin\alpha_1 - 1 & \varepsilon_{23} = \varepsilon_{32} = \dfrac{b_1}{2b_0}\cos\alpha_1 \\ * & * & \varepsilon_{33} = \dfrac{c_1}{c_0} - 1 \end{bmatrix},$$

where the subscript 0 or 1 denotes the unstrained or the strained unit cell, and the asterisk (*) indicates that the matrix is symmetric about the diagonal. Once the strain tensors with respect to the crystal [100]-[010]-[001] coordinate system are determined, the corresponding full stress tensors with respect to the same coordinate system can be calculated based on the stiffness matrix of Si.[17]

Three widely separated positions (denoted as A, B, and C) along the wire were studied. The full strain and stress tensors with respect to the crystal coordinate system were then transformed to the sample coordinate system (x-y-z). The strain and stress tensors were then diagonalized to obtain the principal strains and principal stresses (see Figs. 1(b) and 1(c)) with their corresponding principal direction vectors (Table S1, supplementary material). It can be seen from Fig. 1(c) that the stresses are all positive along the principal directions, and up to ~0.8 GPa of tensile stress has been established inside the Si. Also, the stresses are relatively uniform along the fiber. The strain can be relaxed after etching out the surrounding silica (Fig. S1, supplementary material), indicating that it originates from the thermal expansion mismatch between the Si and silica during cooling. This three-dimensional anisotropic tensile stress state is rather unusual for Si.

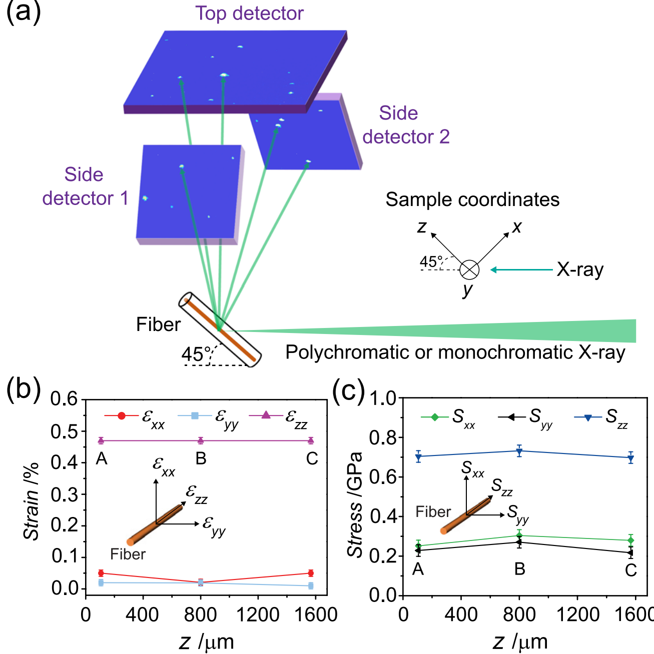

FIG. 1. Characterization of strain and stress using synchrotron micro-beam X-ray diffraction microscopy. (a) Schematic of the experimental setup using which the Laue diffraction patterns are collected by three area detectors. (b) and (c) Principal strains and stresses are all positive at different locations along the fiber.

In order to predict to which extent the electronic band structure changes under this strain state, we performed density-functional theory (DFT) calculations using the Quantum-Espresso distribution[18] within an optimally tuned Perdew–Burke–Ernzerhof hybrid exchange-correlation approximation (PBE0). The exchange mixing fraction of the PBE0 functional was deliberately decreased from its original value of 25% to 12% so as to reproduce the experimental band gap of Si at zero strain (zero strain corresponding to the equilibrium lattice spacing of Si for the corresponding model functional), following a similar approach as that justified in Ref. 19. Norm-conserving pseudopotentials were used throughout with a kinetic energy cutoff of 40 Ry and a charge density cutoff of 160 Ry. The experimentally determined full strain tensor in the crystal coordinate system was used as the input. As shown in Fig. 2, at the experimental strain, both the conduction band minima and the valence band maxima are lowered, and a 30 meV indirect band gap reduction is predicted. Split-orbit coupling was not considered in the calculations. Therefore, the heavy-hole (HH), light-hole (LH), and split-off (SO) bands are degenerate at the Γ point for the unstrained state (blue lines). However, these valence bands start to split slightly under the experimental strain due to their anisotropic nature, as can be seen in the right panel in Fig. 2.

The bandgap shift was also experimentally observed through energy-dependent quantum efficiency measurement. The Si wire was etched out of the two ends of the silica capillary using 48% buffered HF acid and contacts were made with aluminum in a thermal evaporator followed by thermal annealing in dry N_2 at 430 °C for 30 min. A Fianium SC-450 supercontinuum laser was used as the excitation source and an acousto-optic tunable filter is used to tune the

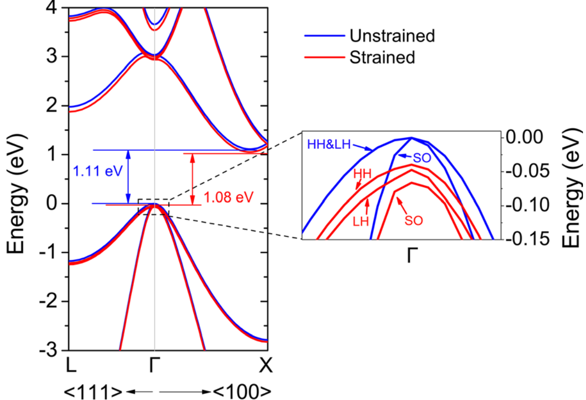

FIG. 2. Electronic band structure calculation of Si free of strain (red) and under the experimental strain (blue) using the density-functional theory (DFT).

29 May 2024 01:12:47

wavelength from 800 nm to 1500 nm. Incident optical power at each wavelength was measured before the measurement and kept low enough to avoid the two-photon absorption effect. When the fiber is illuminated with an 800 nm laser light, the current increases dramatically, indicating that the fiber is photosensitive (Fig. 3(a)). The quantum efficiency Y of both the Si fiber and a Si wafer reference (resistivity of 1700 Ω·m from MTI Corp.) was studied as a function of excitation photon energy, where Y is defined by the following equation:[20]

$$Y = \frac{I_{ph} \cdot E_{ph}}{q \cdot P},$$

where I_{ph}, P, E_{ph}, and q are the net photocurrent, optical power at each wavelength, corresponding incident photon energy, and electric charge, respectively. As the photon energy decreases towards the band edge, the quantum efficiency Y also decreases, because the available density of states for electronic transition decreases.[21] The square root of the measured quantum efficiency, which is considered to be directly proportional to the absorption coefficient,[22] for both the Si microwire and the Si wafer is plotted as a function of photon energy, as shown in Fig. 3(b). The band gap energy for the Si wafer is determined to be ∼1.12 eV, which is consistent with the value typically determined from absorption coefficients (supplementary material Fig. S3). Plotting it on a log scale helps us to visualize more clearly the band edge shift of the microwire. It shows that there is a ∼50 meV reduction in the band gap as compared with a bulk Si wafer reference, which matches well with the DFT calculation. We noted that the optical phonon energy in Si for the indirect transition is about 50 meV,[23] which makes the Si wafer band edge seem to be about 50 meV smaller than 1.12 eV on a log scale.

Although the experimental strain is not large enough to change the band structure significantly, we investigated the effect of increasing the magnitude of the strain by a multiplicative factor M varying from 1 to 10 using DFT calculations. As can be seen from Fig. 4(a), the energy separation between the light-hole, heavy-hole, and split-off bands of Si at the Γ point are further increased when the strain is increased by a factor of 10. The discontinuity of the bands at the X high symmetry point in the Brillouin zone arises from the fact that the two points immediately to the left and immediately to the right of X are not symmetry-equivalent when the crystal is strained according to experimental conditions (X point and X_1 point are symmetry-equivalent when the crystal is unstrained, and by our definition they are at $0.5\boldsymbol{b}_1 + 0.5\boldsymbol{b}_3$ and $0.5\boldsymbol{b}_1 + 0.5\boldsymbol{b}_2$ in the reciprocal space, respectively, where $\boldsymbol{b}_1$, $\boldsymbol{b}_2$, and $\boldsymbol{b}_3$ are the primitive reciprocal lattice vectors[24]). Both the conduction band and valence band energies are lowered, but the conduction bands move more and the band minima are now at the X_1 point instead of at $0.85(2\pi/a)$ along the Δ directions,[25] where a is the crystal lattice constant. This causes the band gap to be reduced by 220 meV as shown in Fig. 4(b), while the nature of the bandgap still remains indirect. Such bandgap reduction indicates the absorption band edge shifts to lower energy, which can be desirable for photovoltaic applications.[26] These results could motivate future exploration of applying external tensile stress to the fiber. Although uniaxial stress has been externally applied to Si nanowires[27] and microribbons,[28] the silicon-in-fiber geometry is beneficial for realizing omnidirectional tensile stress[29] when externally stretching the fiber because of the following: first, silica bonds strongly to Si so that large tensile stress can be transferred; secondly, silica has a smaller Poisson's ratio than Si (0.17 vs. 0.27) so that it shrinks less than Si in the transverse direction (perpendicular to the fiber axis), which can effectively induce tensile stress to the Si. Additionally, at larger negative pressure, Si-Si bonds stretch significantly, which could also allow for the exploration of possible polymorphs of Si.[29]

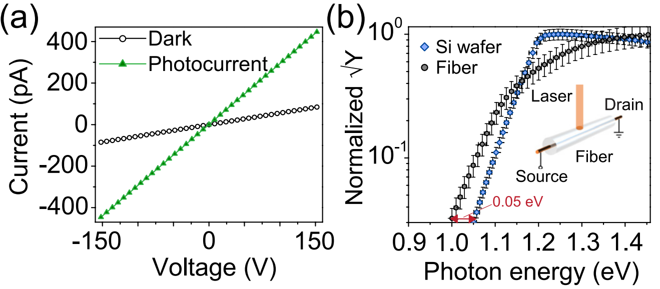

FIG. 3. Electrical characterization of the single crystal Si wire. (a) Photocurrent measurement showing that the wire is electrically conductive and photosensitive. (b) Energy dependent measurement showing that the bandgap of the wire is red-shifted due to strain.

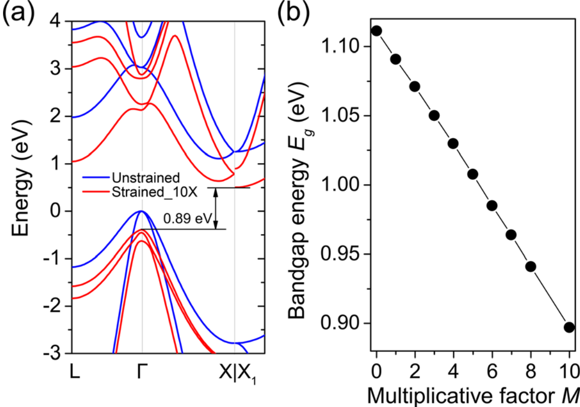

FIG. 4. DFT prediction of (a) the electronic band structure of the Si crystal when the strain magnitude is increased by a factor of 10 (red lines) and (b) the bandgap energy as a function of the multiplicative factor M used to increase the magnitude of the experimental strain.

In summary, we have fabricated single-crystal Si microwires in a silica capillary and the full strain states have been determined through synchrotron X-ray micro-Laue diffraction. An unusual three-dimensional anisotropic tensile stress state is realized in the Si microwire. Due to the single-crystalline nature of the microwire, we conducted DFT calculation for the electronic band structure of the strained microwire based on the experimentally determined strain tensor and the bandgap energy was found to be reduced by 30 meV, in direct accordance with the energy-dependent photoconductivity measurement. External stresses can be applied in the future to further explore fundamental properties of the in-fiber Si, which could ultimately lead to interesting fiber-based optoelectronic devices.

29 May 2024 01:12:47

See supplementary material for details of the principal strains and stresses directions (Table S1), the Raman spectrum of the relaxed microwire (Fig. S1), the characteristic Laue diffraction pattern (Fig. S2), the determination of Si wafer band gap energy (Fig. S3), and the calculated Raman spectra of the strained microwire (Fig. S4).

We acknowledge primary financial support from the Penn State Materials Research Science and Engineering Center for Nanoscale Science, Grant No. DMR 1420620, and partial support from Grant No. DMR 1107894. Use of the Advanced Photon Source was supported by the U.S. Department of Energy, Office of Science, Office of Basic Energy Sciences, under Contract No. DE-AC02-06CH11357. X. Ji and V. Gopalan would like to thank beamline 34-ID-E at the Advanced Photon Source for providing the facilities for diffraction experiments.

[1]C. Kisielowski, J. Kruger, S. Ruvimov, T. Suski, J. W. Ager, E. Jones, Z. Liliental-Weber, M. Rubin, E. R. Weber, M. D. Bremser, and R. F. Davis, Phys. Rev. B **54**, 17745 (1996).
[2]M. L. Lee, E. A. Fitzgerald, M. T. Bulsara, M. T. Currie, and A. Lochtefeld, J. Appl. Phys. **97**, 11101 (2005).
[3]S. E. Thompson, M. Armstrong, C. Auth, M. Alavi, M. Buehler, R. Chau, S. Cea, T. Ghani, G. Glass, T. Hoffman, C.-H. Jan, C. Kenyon, J. Klaus, K. Kuhn, Z. Ma, B. Mcintyre, K. Mistry, A. Murthy, B. Obradovic, R. Nagisetty, P. Nguyen, S. Sivakumar, R. Shaheed, L. Shifren, B. Tufts, S. Tyagi, M. Bohr, and Y. El-Mansy, IEEE Trans. Electron Devices **51**, 1790 (2004).
[4]R. S. Jacobsen, K. N. Andersen, P. I. Borel, J. Fage-Pedersen, L. H. Frandsen, O. Hansen, M. Kristensen, A. V. Lavrinenko, G. Moulin, H. Ou, C. Peucheret, B. Zsigri, and A. Bjarklev, Nature **441**, 199 (2006).
[5]S. F. Feste, J. Knoch, S. Habicht, D. Buca, Q.-T. Zhao, and S. Mantl, Solid-State Electron. **53**, 1257 (2009).
[6]S. F. Feste, J. Knoch, D. Buca, and S. Mantl, Thin Solid Films **517**, 320 (2008).
[7]N. Healy, S. Mailis, N. M. Bulgakova, P. J. A. Sazio, T. D. Day, J. R. Sparks, H. Y. Cheng, J. V. Badding, and A. C. Peacock, Nat. Mater. **13**, 1122 (2014).
[8]K. Kůsová, P. Hapala, J. Valenta, P. Jelínek, O. Cibulka, L. Ondič, and I. Pelant, Adv. Mater. Interfaces **1**, 1300042 (2014).
[9]W. L. Ng, M. A. Lourenco, R. M. Gwilliam, S. Ledain, G. Shao, and K. P. Homewood, Nature **410**, 192 (2001).
[10]J. J. Wortman and R. A. Evans, J. Appl. Phys. **36**, 153 (1965).
[11]R. H. Baughman, J. M. Shacklette, A. A. Zakhidov, and S. Stafström, Nature **392**, 362 (1998).
[12]X. Ji, S. Lei, S.-Y. Yu, H. Y. Cheng, W. Liu, N. Poilvert, Y. Xiong, I. Dabo, S. E. Mohney, J. V. Badding, and V. Gopalan, ACS Photonics **4**, 85 (2017).
[13]P. J. A. Sazio, A. Amezcua-Correa, C. E. Finlayson, J. R. Hayes, T. J. Scheidemantel, N. F. Baril, B. R. Jackson, D.-J. Won, F. Zhang, E. R. Margine, V. Gopalan, V. H. Crespi, and J. V. Badding, Science **311**, 1583 (2006).
[14]W. R. Busing and H. A. Levy, Acta Crystallogr. **22**, 457 (1967).
[15]L. E. Levine, C. Okoro, and R. Xu, IUCrJ **2**, 635 (2015).
[16]J. L. Schlenker, G. V. Gibbs, and M. B. Boisen, Acta Crystallogr., Sect. A **34**, 52 (1978).
[17]M. A. Hopcroft, W. D. Nix, and T. W. Kenny, J. Microelectromech. Syst. **19**, 229 (2010).
[18]P. Giannozzi, S. Baroni, N. Bonini, M. Calandra, R. Car, C. Cavazzoni, D. Ceresoli, G. L. Chiarotti, M. Cococcioni, I. Dabo, A. D. Corso, S. de Gironcoli, S. Fabris, G. Fratesi, R. Gebauer, U. Gerstmann, C. Gougoussis, A. Kokalj, M. Lazzeri, L. Martin-Samos, N. Marzari, F. Mauri, R. Mazzarello, S. Paolini, A. Pasquarello, L. Paulatto, C. Sbraccia, S. Scandolo, G. Sclauzero, A. P. Seitsonen, A. Smogunov, P. Umari, and R. M. Wentzcovitch, J. Phys.: Condens. Matter **21**, 395502 (2009).
[19]J. H. Skone, M. Govoni, and G. Galli, Phys. Rev. B **89**, 195112 (2014).
[20]S. M. Sze and M. K. Lee, *Semiconductor Devices, Physics and Technology*, 3rd ed. (Wiley, Hoboken, NJ, 2012).
[21]D. A. Neamen, *Semiconductor Physics and Devices* (McGraw-Hill, 2012).
[22]H. Helmers, C. Karcher, and A. W. Bett, Appl. Phys. Lett. **103**, 32108 (2013).
[23]J. I. Pankove, *Optical Processes in Semiconductors* (Dover, 1975).
[24]W. Setyawan and S. Curtarolo, Comput. Mater. Sci. **49**, 299 (2010).
[25]Y. Sun, S. E. Thompson, and T. Nishida, J. Appl. Phys. **101**, 104503 (2007).
[26]C. Rödl, T. Sander, F. Bechstedt, J. Vidal, P. Olsson, S. Laribi, and J.-F. Guillemoles, Phys. Rev. B **92**, 45207 (2015).
[27]H. Zhang, J. Tersoff, S. Xu, H. Chen, Q. Zhang, K. Zhang, Y. Yang, C.-S. Lee, K.-N. Tu, J. Li, and Y. Lu, Sci. Adv. **2**, e1501382 (2016).
[28]D.-Y. Khang, H. Jiang, Y. Huang, and J. A. Rogers, Science **311**, 208 (2006).
[29]F. Zhang, D. S. Stojkovic, and V. H. Crespi, Appl. Phys. Lett. **97**, 121906 (2010).

29 May 2024 01:12:47